Utah State University
DigitalCommons@USU

All Physics Faculty Publications | Physics

2007

Electron-Induced Electron Yields of Uncharged Insulating Materials

Ryan Carl Hoffmann
Utah State University

JR Dennison
Utah State Univerisity

Jennifer Albretsen

Follow this and additional works at: https://digitalcommons.usu.edu/physics_facpub

Part of the Physics Commons

Recommended Citation

Ryan Hoffmann and JR Dennison, "Electron-Induced Electron Yields of Uncharged Insulating Materials" Proceedings of the 10th Spacecraft Charging and Technology Conference, (Biarritz, France, June 18-21, 2007). 14 pp.

This Presentation is brought to you for free and open access by the Physics at DigitalCommons@USU. It has been accepted for inclusion in All Physics Faculty Publications by an authorized administrator of DigitalCommons@USU. For more information, please contact dylan.burns@usu.edu.

Electron-Induced Electron Yields of Uncharged Insulating Materials

Ryan Hoffmann, JR. Dennison and J. Albretsen
Utah State University Physics Department UMC 4415
Logan, Utah 84322 USA

Abstract---*This study presents electron-induced electron yield measurements from high-resistivity, high-yield materials to validate a model for the yield of uncharged insulators. These measurements are accomplished by using a low-fluence, pulsed incident electron beam and charge neutralization to minimize charge accumulation. Our measurements show large changes in total yield curves and yield decay curves, even for incident electron fluences of <3 fC/mm^2. We model the evolution of the yield as charge accumulates in the material in terms of electron re-capture based on the extended Chung-Everhart model of the electron emission spectrum. This model is used to explain anomalies measured in high yield ceramics, and to provide a method for determining the uncharged yield in highly insulating, high yield materials. Relevance of these results to spacecraft charging will also be discussed.*

1. Introduction

The central theme of spacecraft charging is how spacecraft interact with the plasma environment to cause charging. Spacecraft accumulate charge and adopt potentials in response to interactions with the plasma environment. Key parameters in modeling spacecraft charging are the electron emission properties of insulating materials, in particular electron yield as a function of incident energy. This determines how much charge will accumulate in spacecraft components in response to incident electron, ion, and photon fluxes. Due to their high mobility, incident electrons play a more significant role in spacecraft charging. However, electron emission in insulators is further complicated by the fact that the yield itself is affected by accumulated surface charge. In order to more accurately model the charging behavior of insulators used on spacecraft, we have developed a model for the yield as a function of surface potential.

In this paper, we present a study of the change in electron induced electron yield that result from the buildup of internal charge distributions due to incident and emitted electron fluxes. Specifically, we look at how charge buildup in highly charging insulating materials affects these fluxes, and their ratio. First, we show an evolution of total, and secondary yield results over a broad range of incident energies in response to accumulated charge for Kapton HN and alumina. Quantifiable changes in yields are observed due to fluences lower than 100 fC/mm^2. We then present a model for the evolution of electron yields as a result of surface charging. This expression is derived from the physics based model for the emission spectrum of secondary electrons developed by Chung and Everhart [6]. This model is fit to measured data to provide electron yields as a function of both incident electron energy and fluence. Using the double dynamic layer model for the internal charge in response to incident charge we develop a model for the electron emission yield as a function of incident charge or equivalently surface potential. Finally, we present an estimate of the "intrinsic" electron yield curve extrapolated to a minimal incident charge.

2. Theoretical Model

2.1 Electron Yield and Emission Spectra

2.1.1 Electron Induced Electron Yield

The total yield, σ, is the ratio of emitted flux to incident flux. By convention, the secondary electron (SE) yield, $\delta(E_o)$, is the ratio for emitted electrons with energy <50 eV and the backscattered electron (BSE) yield, $\eta(E_o)$, is the ratio for emitted electrons with energy >50 eV. An electron yield curve on gold shows the yield as a function of incident electron energy (see Fig 1a). The total yield curve can be characterized in terms of five parameters [9]: (i and ii) the first and second crossover energies, E_1 and E_2, occur when the total yield is equal to unity and no net charge is deposited; (iii and iv) the yield peak, σ_{max}, is the maximum yield and occurs between the crossover energies at E_{max} (The maximum yield is typically found between $200<E_{max}<1000$ eV.); and (v) the rate at which the yield approaches the asymptotic limit, $\sigma \rightarrow 0$, with increasing beam energy, $E_o \rightarrow \infty$.

The electron emission properties of conductors are relatively easy to measure, because emitted electrons are easily replaced by connecting the material to ground [1,2]. However, yield measurements on dielectrics are more difficult because of the response in the yield to charge accumulation [3,5]. Accumulated charge in insulators interacts with incident charged particles through Coulomb interactions and affects electron emission in all three stages of emission models as reviewed in Thompson [3]. Surface potentials resulting from the accumulated charge can affect yields by altering incident (or landing) energies, by affecting the escape energies of secondary electrons (SEs) and backscattered electrons (BSE) or by reattracting low energy SE to a positive charged surface.

For example, Fig 3a shows a very low fluence yield curve taken on alumina, a highly charging material with a combination of high yield and high resistivity. It is easy to see that charging plays a significant role in the shape of the yield curve. Despite using very small incident fluences, the area between the peaks suggests that significant charging is nonetheless being induced. This, in turn, lowers the yield by reattracting some fraction of the SE. This duel-peak behavior is only seen in our system on insulators with σ_{max} > ~5. This is due to the fact that higher yields require less incident flux to induce charging and that highly resistive materials do not dissipate significant charge on the time scale of the measurement.

2.1.2 Electron Emission Spectra Related to Total Yield

Of primary concern of this study is the prediction and measurement of the electron induced electron yield, but we must first turn to the electron emission spectrum to get a clearer view of how charge accumulation effects the yield. Chung and Everhart [6] provide a useful model for the electron emission spectra, which expresses the energy distribution of the number of emitted SE per unit energy in terms of the work function for metals [2]. In the case of insulators, the literature supports a simple substitution of work function by the electron affinity, χ [3]

$$\frac{dN(E;E_o)}{dE} = \frac{k}{E_o}\frac{E}{(E+\chi)^4} \qquad \textbf{[1]}$$

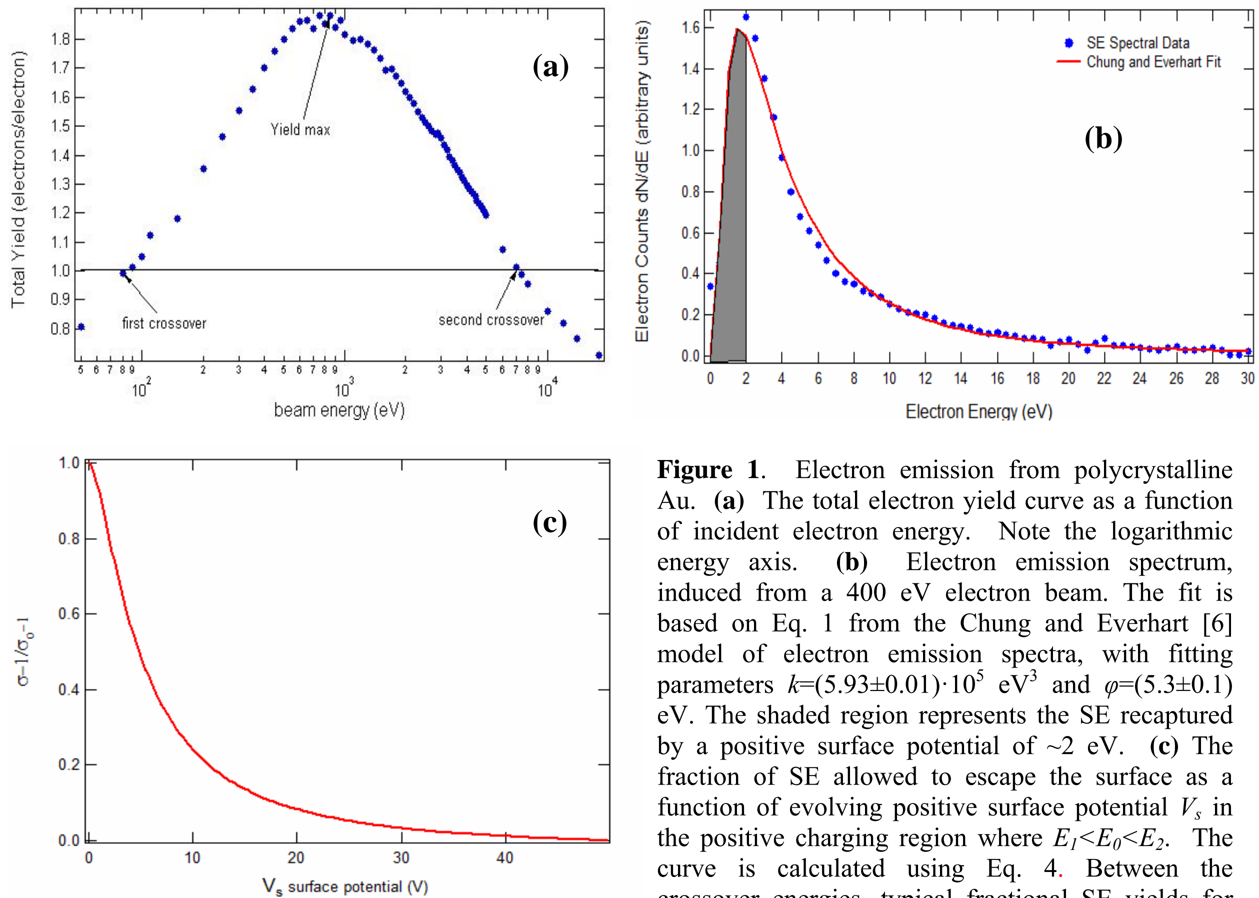

Figure 1. Electron emission from polycrystalline Au. **(a)** The total electron yield curve as a function of incident electron energy. Note the logarithmic energy axis. **(b)** Electron emission spectrum, induced from a 400 eV electron beam. The fit is based on Eq. 1 from the Chung and Everhart [6] model of electron emission spectra, with fitting parameters k=(5.93±0.01)·10^5 eV^3 and φ=(5.3±0.1) eV. The shaded region represents the SE recaptured by a positive surface potential of ~2 eV. **(c)** The fraction of SE allowed to escape the surface as a function of evolving positive surface potential V_s in the positive charging region where $E_1<E_0<E_2$. The curve is calculated using Eq. 4. Between the crossover energies, typical fractional SE yields for insulators approach values of 0.2-0.6, corresponding to positive surface potentials of 3-8 V.

where *N(E)* is the number of emitted electrons, *E* is the SE emission energy, *k* is a material-dependent proportionality constant, and E_o is the incident beam energy. The SE yield in terms of *N(E)* is given by

$$\int_{0eV}^{50eV} \frac{dN(E;E_o)}{dE} dE = \delta_o(E_o) + \eta_o - 1 = \sigma_o(E_o) - 1 \qquad \textbf{[2]}$$

Measured emission spectra for Au are shown in Fig 1b, along with a fit based on the Chung-Everhart model. Between the total-yield crossover energies, E_1 and E_2, the magnitude of insulator charging is positive (since the total yield is greater than one), and the insulator attains a steady-state surface potential of just a few volts positive. This positive charging increases the insulator surface potential barrier by an amount eV_s, where V_s is the positive surface potential. Hence, the resulting secondary electron yield emitted from a positively charged specimen can be expressed as an integral of the uncharged spectrum (taken at the same incident energy) with the integration limits extending from the positive surface potential up to the arbitrary 50 eV limit of SE energy [7,8]:

$$\int_{eV_s}^{50\,eV} \frac{dN(E;E_o)}{dE} dE = \delta(E_o;V_s) + \eta_o - 1 = \sigma(E_o;V_s) - 1 \qquad \textbf{[3]}$$

This integral can be solved analytically by direct substitution of Eq. 1 into Eq. 3 as

$$\int_{eV_s}^{50eV} \frac{dN(E;E_o)}{dE} dE = \frac{k}{6E_o}(h(eV_s,\chi) - h(50eV,\chi))$$

where **[3b]**

$$h(\alpha,\chi) \equiv \frac{3\alpha+\chi}{(\alpha+\chi)^3}$$

This is illustrated in Fig 1b, where the positive surface charging inhibits the escape of lower-energy SE's, thus suppressing the lower-energy portion of the SE spectrum (represented by the shaded area in the figure). Consequently, only the unshaded area of the electron energy spectrum (above eV_s) contributes to the charged electron yield. It follows that the fraction of the SE yield escaping the surface is

$$\frac{\sigma(E_o;V_s)-1}{\sigma_o(E_o)-1} = \frac{\int_{eV_s}^{50\,eV} \frac{dN(E;E_o)}{dE} dE}{\int_{0\,eV}^{50\,eV} \frac{dN(E;E_o)}{dE} dE} = \frac{h(eV_s;\chi) - h(0eV;\chi)}{h(50eV;\chi) - h(0eV;\chi)} \qquad \textbf{[4]}$$

As illustrated in Fig 1c expression 4 gives the fraction of the generated SE that have enough energy to overcome the surface potential and contribute to the yield. For charged insulators, this is the fraction of secondary electrons that escape the intrinsic electron affinity and the positive surface potential created by incident charge. Using the fact that the total yield is the sum of secondary and backscatter yields we can solve Eq. 3 for the secondary yield in terms of V_s.

$$\sigma - 1 = (\sigma_o - 1)H(V_s;\chi) = \delta(V_s) + \eta_o - 1 \qquad \textbf{[5]}$$

where

$$H(V_s;\chi) \equiv \frac{h(eV_s;\chi) - h(50eV;\chi)}{h(0eV;\chi) - h(50eV;\chi)}$$

Using Eq. 5 and solving for $\delta(V_s)$ gives

$$\delta(V_s;\chi) = (\sigma_o - 1)H(V_s;\chi) - \eta_o + 1 \qquad \textbf{[6]}$$

This gives us an expression for the SE yield as a function of surface potential where $\sigma(E_o)$ is the uncharged total yield, in practice this becomes the minimally charged yield. This expression then becomes a one parameter fit χ for the SE yield as positive surface potential is increased and SE are reattracted. This phenomenon has been termed secondary yield decay. In order to proceed, we need to develop a specific expression for the surface potential V_s as a function of incident charge Q_o, as it appears in the lower limit of the integral in Eq. 4.

2.2 Charge Distribution in Insulators

Let us consider a succession of more sophisticated charge distributions. For the purposes of this study we will focus only on the incident electron energies between the crossover energies (ie positive charging regime). For biased conducting materials, the charge resides near the surface in accordance with Gauss' law. For ideal insulators, one assumes that primary electrons (PE) do not move appreciable distances within the material and that the SE charge distribution is the same as the production profile. The simplest model of charge distribution in an insulator is that all incident charge is deposited in a simple thin layer at a depth equal to the penetration depth of the primary electron, $R(E_o)$. This follows from the Bethe approximation for SE production used in the Sternglass formulation of the yield formula [11,12].

To first order, we can model the charge deposition as a single infinite charge layer at the surface of a sample of thickness D. Using a parallel plate capacitor model with the total electron yield dependence included gives

$$V_S = \frac{Q_o(\sigma - 1)\, D}{\varepsilon_o\ \varepsilon_r\ A_o} \quad \textbf{[7]}$$

As expected, for Eq 7 V_s is positive (negative) for σ grater (less than) unity and in the limit were $\sigma \rightarrow 1$ no charging occurs. While this model provides a useful first order approximation for the surface potential it is rather simplistic in its treatment of the internal charge distribution. Finite resistivity allows redistribution of charge within the insulator, leading to more complicated internal charge distributions [13]. Previous models of insulators have shown that the internal charge distributions (both evolving distributions as well as static charge distributions), resulting from incident electron irradiation, form multiple alternating positive and negative charge layers [9,10], [14–17]. Measurements of internal charge distributions of thin-film insulators confirm the general nature of these distributions [18–20]. Thomson provides a useful review of the literature on charge distributions within insulators, with application to electron emission from insulators [3]. Net positive (negative) charge will build up when the total number of electrons leaving the insulator sample is greater than (less than) the total number of incoming electrons. However, the spatial and charge-polarity configurations of these layers can be complex and difficult to predict; the distributions can depend on a number of factors that include the magnitude of electron yield, electron yield crossover energies (particularly E_2), material resistivity (both innate and radiation-induced conductivity), dielectric strength, electron trapping and detrapping rates, incident electron penetration depths, mean SE escape depths, and incident electron fluxes and energies. The combination of these layers is what defines the overall magnitude of the surface potential.

Between the crossover energies, incident electron penetration is only somewhat larger than the SE escape depth, resulting in a small deep negative charge region and a larger positive charge region closer to the surface (see Fig. 2). The electric field from the negative charge again retards further incident electron penetration and acts to drive more low-energy SEs from the sample, thereby enhancing the positive charge region [5, 8]. The electric field from the positive charge region, in turn, acts to reattract the lowest energy SE emitted from the surface (gray region in Fig. 1b), thereby establishing a shallow negative surface charge region. A double-charge distribution (positive–negative) is formed where the positively charged region, from SE depletion, occurs between the surface and λ_{SE} and a negatively charged region, from embedded incident electrons, occurs between the surface and R.

For this charging scenario, the dynamic double layer model (DDLM) has been presented in the literature [14, 15, 21] to predict ensuing internal electric fields and potentials. For the DDLM charge distribution deposited over a thickness, the surface potential can be approximated assuming a parallel-pate capacitor geometry with total incident charge Q_o as [3, 16]

$$V_S = \frac{Q_o(\sigma-1)\,D}{\varepsilon_o\,\varepsilon_r\,A_o} - \frac{\sigma\,Q_o\,\lambda_{SE} + Q_o\,R}{2\,\varepsilon_o\,\varepsilon_r\,A_o} = \frac{Q_o D}{\varepsilon_o \varepsilon_r A_o}[(\sigma-1) - \sigma\frac{\lambda_{se}}{2D} - \frac{R}{2D}] \qquad \textbf{[8]}$$

The first term is from the net charge distribution of magnitude $Q_o(\sigma-1)$ give by Eq 7, the term involving λ_{se} is for the positive charge distribution of magnitude $Q_o\sigma$ from SE emission, and the term involving R is for the imbedded PE distribution of magnitude Q_o. The thin-film capacitor geometry is a reasonable approximation since charge deposition area A_o, which is given by the electron beam radius R_{beam}, is much greater than D, R, and λ_{SE} (for studies reported here, R_{beam} was on the order of 1.5 mm, whereas insulator thicknesses ranged from 5 μm to 1 mm). Furthermore, it can be seen that the first term in Eq. 8 dominates if the insulator thickness D is much greater than R or λ_{SE} (R did not exceed ~1 μm for the incident energies reported here); this approximation is equivalent to assuming a uniform charge distribution, as given in Eq.7. Notice that V_s is also a function of the total yield $\sigma(Q_o)$, which itself is dependant on incident charge.

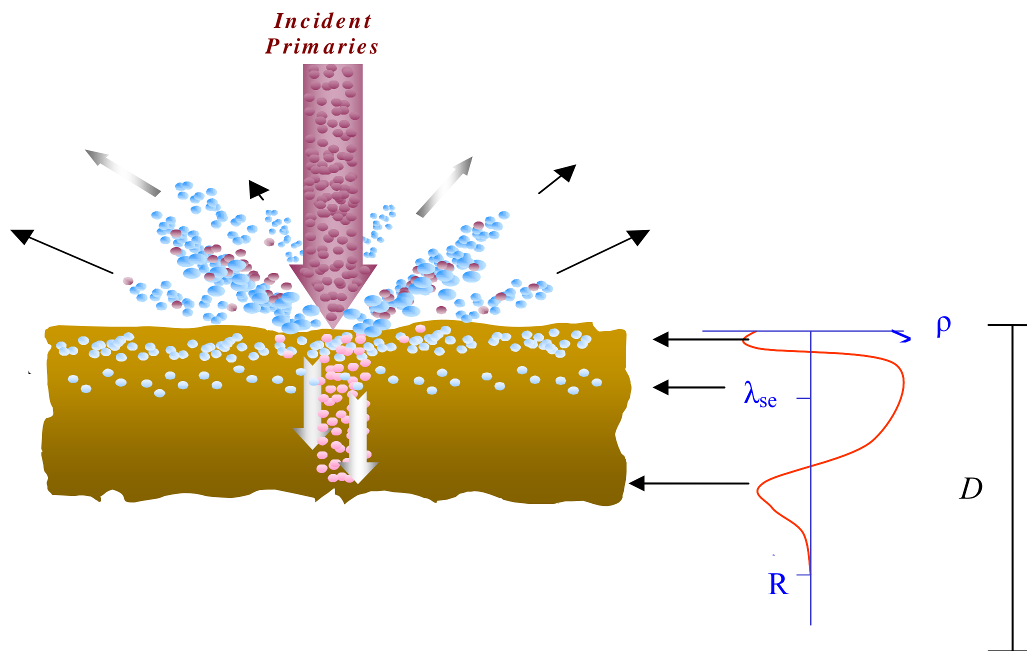

Figure 2. (Left) Standard models of electron emission divide the process into three stages: production, SE transport and escape. Primary electrons (PE) of energy E_o impinge on the surface and penetrate up to a depth R. Secondary electrons (SE) are produced within the material and some are transported to the surface. The Secondary electron escape depth λ_{se} is also shown. A fraction of these electrons can overcome the surface barrier and escape. In the case of positive surface potential some secondarys are reattracted and form a shallow negative layer. **(Right)** Schematic of a typical internal charge distribution for $E_1<E_o<E_2$ with $\sigma>1$ and overall positive charging. Note the negative charge regions near the surface due to the reattracted electrons, the positive charging region due to SE emission and the embedded PE deep within the material. Material thick ness is given by D and there is assumed a grounded conductive backing.

2.3 Response of Total Yield to Evolving Surface Potential

We can now combine our expression for the electron yield in terms of the Chung-Everhart model of electron emission (Eq. 2-6) with a model of the surface voltage in terms of incident charge from the DDL model (Eq. 8) to derive a model for the evolution of the yield in response to positive surface potential. Both of these component models are physics based and have been experimentally validated. In order to proceed, and combine these two expression, we need to make several assumptions.

- The distribution of emitted electrons given by Eq. 1 does not change shape with charge accumulation, but only changes amplitude and shifts peak position. Experimental evidence for both biased conductors and charged insulators suggests this is a reasonable assumption [5, 7].
- The BSE yield is assumed to be unaffected by the positive surface potential developing on the sample. This is reasonable as long as the incident energies are much greater than the surface potential. In the positive charging regime this is true because the surface potential is never more that about +20 eV, and usually only a few eV. Further, We assume that the BSE yield is independent of incident electron energy, that is $\eta(E_o) \rightarrow \eta_o$.
- No significant charge is leaking though the sample to ground on the time scale of our measurements. This is reasonable, given that the bulk resistivity of 10^{17} ohm/cm corresponding to a charge decay time of several hours, whereas the measurements take only seconds.

While these assumptions make the derivation possible we still encounter considerable difficulty when merging these two models. In order to get an expression for measured data δ vs. accumulated incident charge or equivalently surface potential, one need only plot $\delta(E_o;V_s)$ vs. $Q_o(V_s)$ with either V_s or Q_o defined implicitly.

3. Experiment

3.1 Instrumentation and Methods

We briefly describe the instrumentation used at Utah State University (USU) to study electron emission from insulators [1]. Electron emission measurements are performed in an ultra-high vacuum chamber (base pressure < 10^{-9} Torr) to minimize surface contamination that can substantially affect emission properties [21,22]. Electron sources provide electron energy ranges from ~50 eV to ~30 keV and incident electron currents (1-100 nA) with pulsing capabilities ranging from 10 ns to continuous emission [1-3]. A hemispherical detector features an aperture for incident electron/ion admission and a fully-encased hemispherical collector for full capture of emitted electrons with a retarding-field analyzer grid system for emitted-electron energy discrimination [2,3,5]. A sample stage holds 11 samples that can be positioned in front of various sources and detectors and is detachable for rapid sample exchange.

A DC method with a continuous, low-current beam of electrons is used to measure electron emission from conducting samples. Charge added to or removed from a conductor via electron emission can be rapidly replaced by connecting the sample to ground [1,2]. Reviews of methods used by previous investigators to study insulator emission are found in Thompson [3] and reference [24]. The fully encased hemispherical grid retarding field detector facilitates high accuracy measurements of absolute yields, on the order of ± 2% for conducting samples, it also

allows the application of bias to each of the discrete elements of the detector. These biases allow for the discrimination of secondary and backscatter electrons and measurement of electron emission spectra. Finally, the individually biased elements of the detector allow for extensive instrument characterization. For conductor measurements, a continuous incident beam is shown on the sample and the currents on all the elements are measured using electrometers. This allows measurement of the total yield. A 50 V bias is then applied to the discriminating grid to allow only the BSE to reach the detector, thus giving the BSE yield. The secondary yield is then the difference of these two measurements. Electron emission spectra used a variable biased grid.

3.1.1 Insulators Electron Yield Measurement Techniques

The system at USU to measure electron emission from insulators uses the same full encased hemispherical grid retarding field detector in concert with methods to control the deposition and neutralization of charge [3,5,23,24]. Typically, charge deposition is minimized by using a low current beam (~5-30 nA) focused on a sample area of ~7 mm^2 that is delivered in short pulses of ~5 μsec. Each such pulse contains ~10^6 electrons/mm^2. The pulsed system uses custom detection electronics with fast (1-2 μs rise time) sensitive/low noise (10^7 V/A / 100 pA noise level) ammeters [3,23]. Charge dissipation techniques include a low energy (~1-10 eV) electron flood gun for direct neutralization of positively charged surfaces and a variety of visible and UV light source for neutralization of negatively charged surfaces through the photoelectric effect [3,5]. Sample heating to ~50-100 °C has also been used for dissipation of buried charge by thermally increasing the sample conductivity.

To measure points on the yield curves at a particular energy, a series of 10 to 50 pulses at constant incident energy are measured with 5-10 sec of neutralization between each pulse, using both low energy electron and visible-ultraviolet flooding. The neutralization technique has been experimentally verified to be an effective method for discharging positive surface potential (see Fig. 3b). Similar series of pulses at fixed incident energy, taken without neutralization, constitute yield decay curves.

3.2 Electron Emission Measurements on Insulators

Using the method described above we have been able to measure yields on insulators with errors of ± 5%. This method has been used to measure insulators with modest resistivity (~10^{15} Ω/cm) and modest σ_{max} (~4). It has also been used for insulators such as kapton with high resistivity (~10^{19} Ω/cm) and modest σ_{max} (~3). As engineering demands become more extreme, so do the demands on the materials, forcing the use of insulators with both higher resistivity and a higher yield. One such material is alumina with a resistivity of ~10^{17} Ω/cm and a E_{max} of ~7. While our methods are effective at dissipating charge, we are limited by how small the incident fluence can be, before the emission signal is lost in the noise. In insulators with modest yield, the incident pulse does not produce enough secondary electrons to appreciably charge the sample; however, in high yield insulators the incident pulse does. This is evident in Fig. 3a: at energies that have a low yield, in the leading and trailing edge of the yield peak, we see little evidence of charging, while in the middle where the yield should be the highest, we see significant charging. Severe undissipated positive charging in the peak energy range causes the yield to be suppressed toward unity, as we would expect for positive surface potential.

To verify the effectiveness of the pulse neutralization method described above, a long series of pulsed measurements at a fixed energy and fluence were taken to look for any change in the yield that would indicate residual potential building up from pulse to pulse. The data

presented in Fig. 3b and does not show any long term change in the total yield. There is < 1% change in the yield over the first 50 pulses that each contain 10^6 electrons. There is a slight upward trend with an ~7% increase in the yield over the full length of the experiment with ~800 pulses and a total incident dose of ~20 fC/mm^2; this is attributed to instrumental drift over the 6 hours it took to obtain this data.

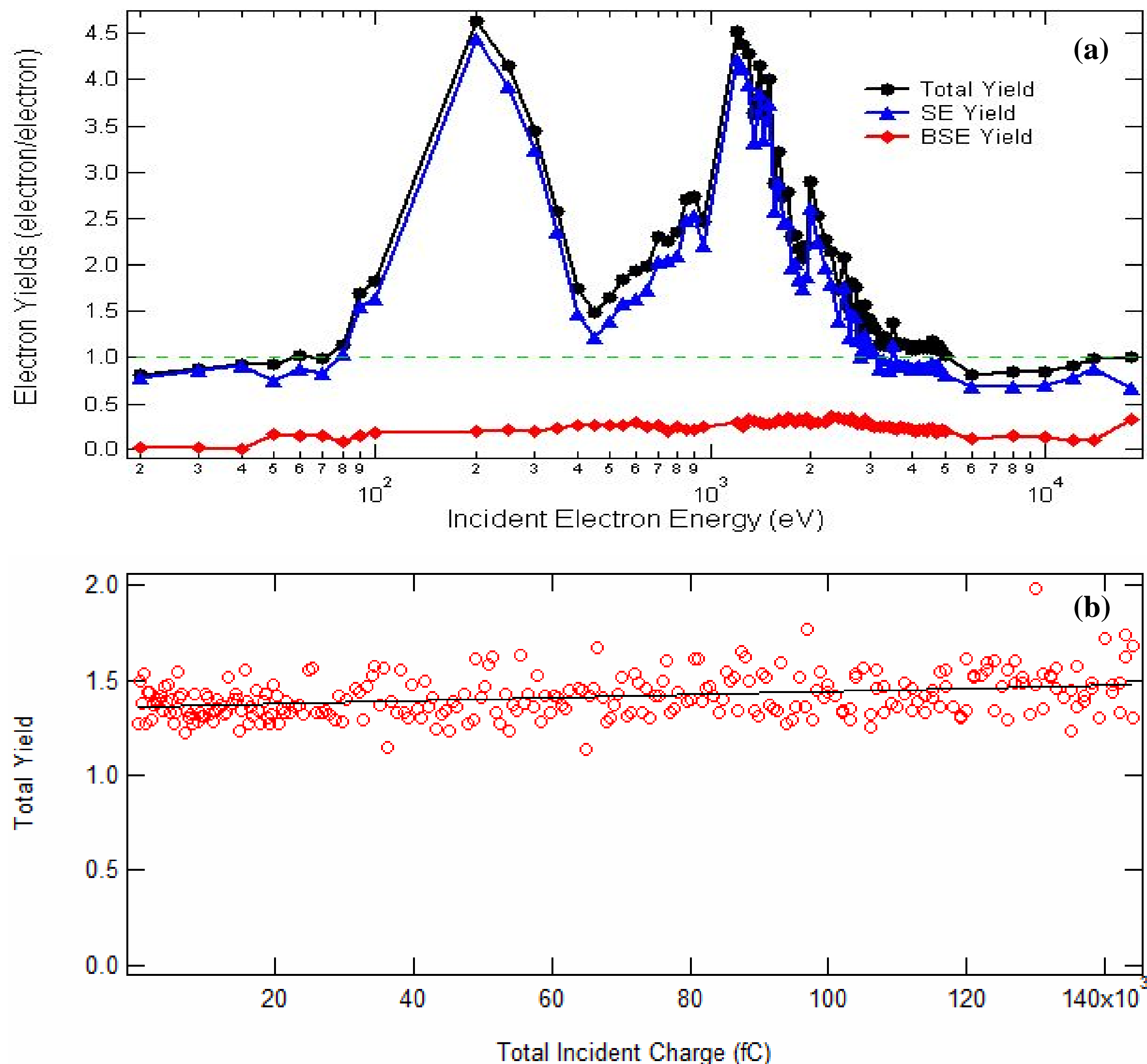

Figure 3. **(a)** Electron induced yield curve from 99.9% pure alumina 1 mm thick. Note the severe depression, due to positive surface charging, in the yield where E_{max} should be. **(b)** Yield measured on 1 mil thick Kapton with 400 eV incident pulses. Discharge methods were employed after each pulse and no significant charging was observed over the entire dose. The slight rise in the yield is due to instrumental drift over the 6 hours needed to collect this data set.

3.2.1 Yield Decay Curves

By measuring a sequence of yields with the method described above, without the discharging between pulses, we generate a yield decay curve. This allows more and more charge to accumulate within the sample with each pulse, thus reattracting more secondary electrons until the yield approaches unity. This is shown in Fig. 4a for alumina. From this data we see a 23%

change in the yield over 50 pulses of 10^6 electrons, as compared to a < 1% change when using neutralization.

3.2.2 Yield Dose Decay Curves

Flooding stops residual potential from affecting the yield from pulse to pulse. However, the question still remains, whether a single incident pulse contains enough electrons to induce significant charging. In other words, is the incident pulse inducing enough charge to appreciably affect the yield? The results of a low fluence measurement of the yield curve seen in Fig 3a, suggests that the pulse *is* affecting the yield. To verify this, the yield was measured as the fluence per pulse was varied (Fig. 4b). In this case the potential was not allowed to accumulate from pulse to pulse as in a typical decay curve. The beam diameter and incident energy were kept constant and only the number of electrons per pulse was varied. It is evident that as the incident fluence decreases, the yield continues to rise. Eventually we reach an instrumental limit cannot make yield measurements at lower fluence pulses. Work is in progress to lower the noise threshold in our system to enable measurements of the minimally charged yield. In the mean time, we have developed less direct methods of measuring the yield curve in the low fluence limit where the pulse does not affect the yield.

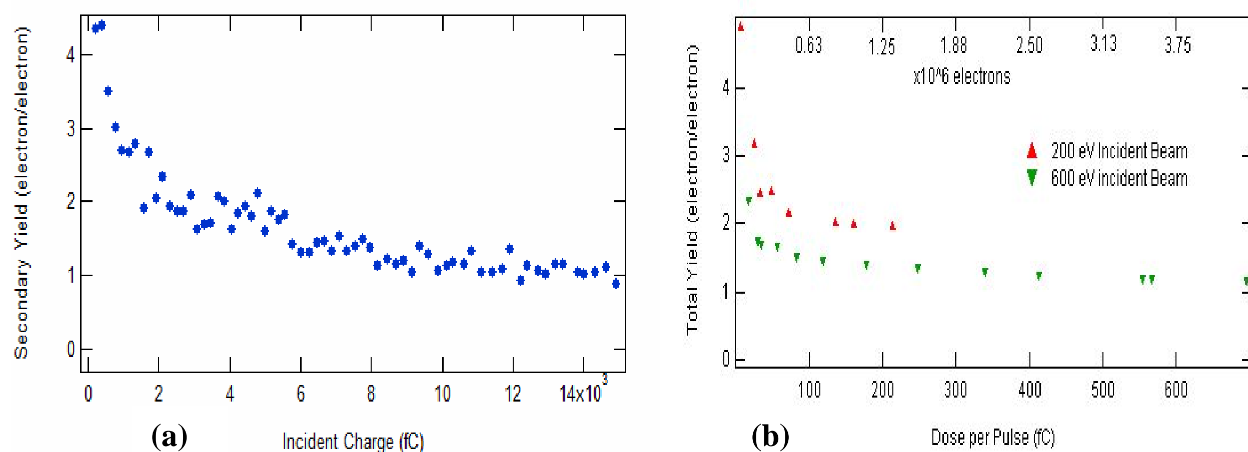

Figure 4. (a) A yield decay curve taken on alumina at an incident energy of 200 eV. These data were taken by not discharging between pulses and allowing the sample potential to build up. **(b)**This dose decay curve was taken on Kapton HN by adjusting the number of electron contained in the incident pulse and keeping all other parameters kept the same. In this range a change of only $4\text{x}10^6$ electrons over 7 mm^2 produces a ~40% increase in the yield. Dose decay curves are shown for both 200 eV and 600 eV incident energies.

3.3 Reconstruction of Uncharged Yield Curve

Measuring the yield for a minimally charged insulator may be possible if the noise in the system can be sufficiently reduced. In the mean time, we propose a method for turning charging to our advantage. In Section 2, we developed a method for determining the dependence of the yield on surface potential. Equation 8 provides a model to calculate surface potential from the cumulated incident charge density. Take together with Eq. 6 and V_s as an implicit variable, these two expressions allow calculation of yield as a function of cumulative charge, that is, the yield decay curves. As mentioned earlier the lower limit in the denominator of Eq. 4 needs to reflect

the residual charge on the surface due to the first pulse. We use the yield measured with this first pulse as $\sigma_o(E_o)$ in Eq. 6. This now provides an expression for the yield as a function of surface potential.

Decay curves were then measured over a spectrum of 21 incident energies ranging from 200 eV to 5000 eV and then fit with Eq.6. A representative energy of 200 eV for alumina as shown in Fig. 5a. (This method of yield measurement is invalid at energies below 200 eV because we can no longer make the assumption that the BSE are not affected by surface potential.) Using these fits to the measured decay curves, we can generate yield curves as a function of incident energy by extracting the yield at a specific cumulative incident charge from each of the family of fitted decay curves for a range of energies to produce a yield curve at that charge.

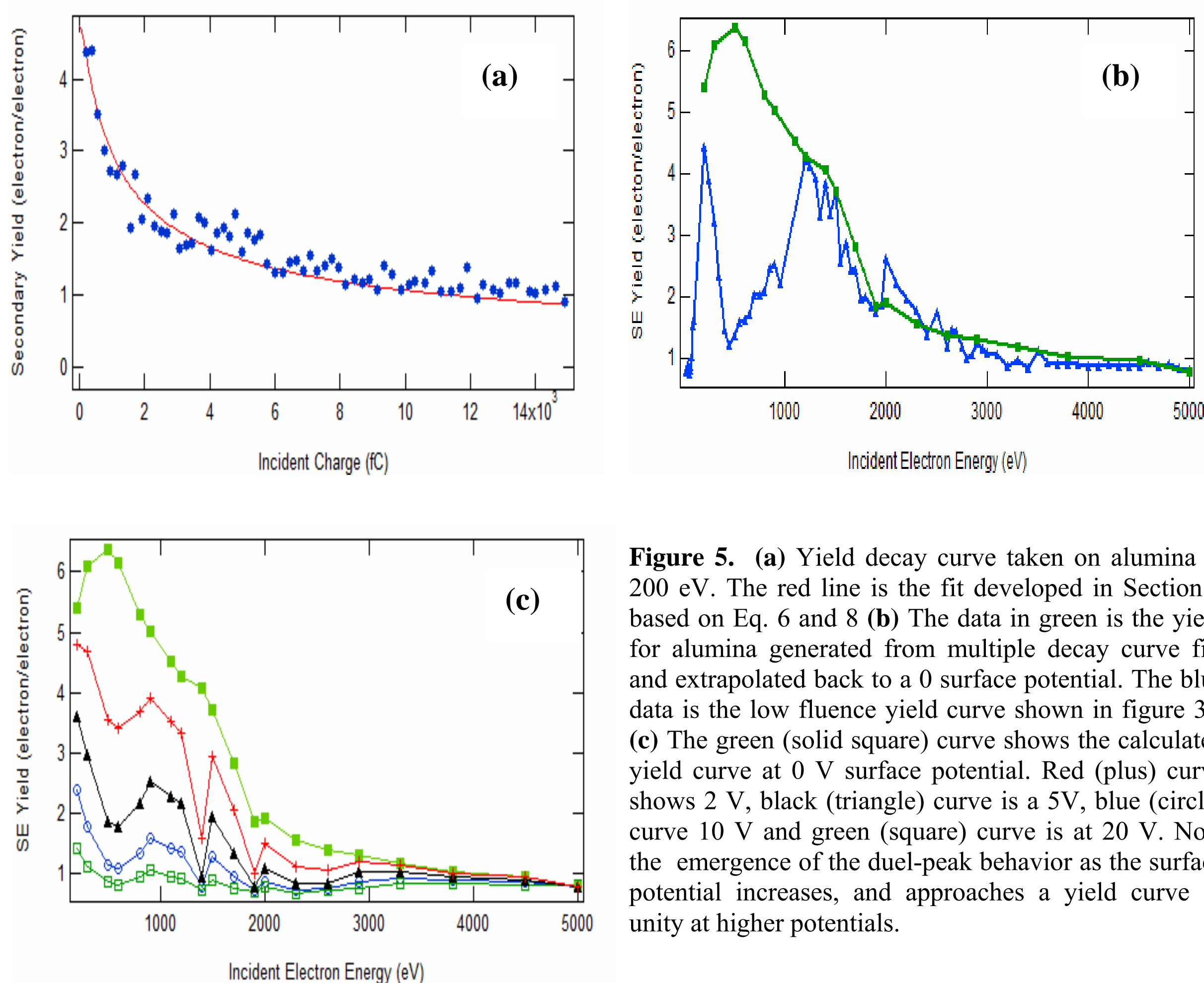

Figure 5. **(a)** Yield decay curve taken on alumina at 200 eV. The red line is the fit developed in Section 2 based on Eq. 6 and 8 **(b)** The data in green is the yield for alumina generated from multiple decay curve fits and extrapolated back to a 0 surface potential. The blue data is the low fluence yield curve shown in figure 3a. **(c)** The green (solid square) curve shows the calculated yield curve at 0 V surface potential. Red (plus) curve shows 2 V, black (triangle) curve is a 5V, blue (circle) curve 10 V and green (square) curve is at 20 V. Note the emergence of the duel-peak behavior as the surface potential increases, and approaches a yield curve of unity at higher potentials.

While this method is very time intensive, it can provide a great wealth of information. We can extrapolate these decay curve fits back to a zero surface potential to generate the "intrinsic" yield curve shown by the green data in Fig. 5b. When compared to the traditional yield curve measurements (blue data in 5b) described in section 3.1, we see that is resolves the charging difficulties, predicts a much higher σ_{max}, and eliminates the double peak behavior. In addition, Fig. 5c shows the yield predicted curves at several representative surface potentials; we see that, as the potential increases, we start to see the emergence of the duel-peak behavior observed in

the traditional low-fluence pulsed method of yield measurement and that at higher surface potential the yield curve approaches unity at all incident energies (see Fig. 3c).

4. Conclusions

The studies described in this paper have demonstrated that pulsed electron methods provide an effective way to measure the "intrinsic" electron emission properties of uncharged insulators. They have also been shown to provide a sensitive tool to explore the effects of accumulated charge from incident electron beams on the electron emission properties of insulators. Indeed, electron emission properties have been shown to be very sensitive to charge accumulation, showing pronounced effects after as little as <50 pC/cm^2 of incident charge. The effect of internal charge accumulation has been quantitatively observed on the secondary yield. Distinct behaviors have also been observed in yield decay curves between the crossover energies, due to the build up of positive charge.

Simple modifications have been made to a physics-based (Chung-Everhart) model for the spectral emission of secondary electrons and coupled with existing simple models for the internal charge distribution resulting from electron emission for insulators. This union has provided an expression that correctly describes the behavior of the secondary yield as positive potential accumulates on the material surface. We have also developed an expression for the yield decay curves, which measure the total yield modifications as a function of cumulative incident charge.

The expressions for fitting the yield decay curves allows us to reconstruct yield as a function of both incident energy and specific incident pulse fluences. We have found good evidence that the duel-peaks observed in the traditional low fluence pulse yield measurement are the result of positive surface charging. This method provides us with a way to make measurement of the uncharged yield in insulators with high resistivity and high yield that would not otherwise be possible.

Two important questions are raised by this study that will be pursed in future work. First, we note that some previous studies of the electron yield curves of high yield, high resistivity insulators using very high fluence beams (many orders of magnitude higher that our study) have measured yield curves similar to our "intrinsic" yield curves, rather that double peak or unity yield curves characteristic of highly charged samples[26,27]. Often such studies use highly focused beams from AES or SEM systems, with beam diameters <1 μm and fluences 10^4-10^7 times higher that our studies. We speculate that the local sample resistivity of the insulator may be reduced due to radiation induced conductivity (RIC) leading to charge dissipation within the sample. We also note that RIC persists for some time after the beam is turned off, so that this explanation could also be applicable to pulsed or rastered probe beams. This explanation is closely related to a study of Green and Dennison [28] of the measurements of resistivity by the charge storage method for an intense, rastered proton beam. The other question that arises is whether our studies of the "intrinsic" and charged insulator yields with low fluence beams are relevant to models of insulators charging and yields in the space environment. One might argue that all insulators will quickly charge to the point that all yields will be unity. Alternately, one might argue that only "intrinsic" yields are relevant for very low space environments fluxes and that only RIC-enhanced yields like those measured with high fluence test apparatus are relevant for high flux space environments. However, it appears, (at least for certain high yield, high resistivity materials used in the construction of spacecraft), that typical ambient space environment fluxes may well produce charging conditions similar to those in our low fluence

yield measurements. The answers to both of these questions are open issues that certainly merit continued study.

5. Acknowledgements

The authors would like to thank J. Abbott, J. Cazaux and O. Jbara for discussions and insight into the problem. This study was partially funded by the NASA Solar Probe Mission through the Johns Hopkins University Applied Physics Laboratory and the NASA Space Environments and Effects program.

6. References

[1] J.R. Dennison, C.D. Thomson, J. Kite, V. Zavyalov, J. Corbridge, "Materials Characterization at USU: Facilities and Knowledgebase of Electronic Properties Applicable to Spacecraft Materials," Proc. 8th Spacecraft Charging Tech. Conf., (Huntsville, AL, USA), 2004.

[2] Nickles, N. E., The Role of Bandgap in the Secondary Electron Emission of Small Bandgap Semiconductors: Studies of Graphitic Carbon, Ph.D. Dissertation, Utah State University, 2002.

[3] C.D. Thompson, "Measurements of Secondary Electron Emission Properties of Insulators," Ph.D. dissertation, Utah State University, Logan, UT, 2004.

[4] JR Dennison, C. D. Thomson, and Alec Sim, "The effect of low energy electron and UV/VIS radiation aging on the electron emission properties and breakdown of thin-film dielectrics," Proceedings of the 8th IEEE Dielectrics and Electrical Insulation Society (DEIS) International Conference on Solid Dielectrics (ICSD), 967-971, (IEEE, Piscataway, NJ, 2004).

[5] Alec Sim, J.R. Dennison and Clint Thomson, "Effects Of Incident Electron Fluence And Energy On The Electron Yield Curves And Emission Spectra Of Dielectrics," *Bull. Am. Phys. Soc.* **50**(1) Part II, (2005).

[6] Chung, M. S., and T. E. Everhart, "Simple calculation of energy distribution of low-energy secondary electrons emitted from metals under electron bombardment," J. Appl. Phys. 45 (2), 707-709 (1974).

[7] N. Nickles, R.E. Davies, J.R. Dennison, "Applications of Secondary Electron Energy- and Angular-Distributions to Spacecraft Charging," Proc. of the 8th Spacecraft Charging Tech. Conf., (AFRL Sc. Center, Hanscom AFB, MA, USA), 2000.

[8] L. Reimer, Scanning Electron Microscopy. Physics of Image Formation and Microanalysis, New York, USA: Springer-Verlag, pp. 119-121, 1985.

[9] Sébastien Clerc J.R. Dennison and Clint Thomson, « Importance of Accurate Computation of Secondary Electron Emission for Modeling Spacecraft Charging," Proceedings of the 9th Spacecraft Charging

[10] X. Meyza, D. Goeuriot, C. Guerret-Piecout, D. Treheux, H.-J. Fitting, "Secondary Electron Emission and Self-consistent Charge Transport and Storage in Bulk Insulators: Application to Alumina," J. Appl. Phys., vol. 94, pp. 5384-5392, 2003.

[11] Sternglass, E. J., "Secondary electron emission and atomic shell structure," Phys. Rev. 80, 925-926 (1950); Sternglass, E. J., An Experimental Investigation of Electron Back-Scattered and Secondary Electron Emission From Solids, Ph.D. Dissertation, Cornell University, 1953.

[12] Young, J. R., "Penetration of electrons and ions in aluminum," J. Appl. Phys. 27 (1), 1-4 (1956).

[13] A. Melchinger, S. Hofmann, "Dynamic double layer model: Description of time dependent charging phenomena in insulators under electron beam irradiation," J. Appl. Phys. vol. 78, pp. 6224-32, 2003.

[14] Cazaux, J., private communications, 2005.

[15] Cazaux, J., K. H. Kim, O. Jbara, and G. Salace, "Charging effects of MgO under electron bombardment and nonohmic behavior of the induced specimen current," J. Appl. Phys. 70 (2), 960-965 (1991); Cazaux, J.,Some considerations on the secondary electron emission δ from e- irradiated insulators," J. Appl. Phys. Vol. 85, pp. 1137-1147 (1999).

[16] Cazeaux, J., "Charging in Scanning Electron Microscopy 'from Inside and Outside'," Scanning, 26, 2004.

[17] Miyake, H., Y. Tanaka, and T. Takada, "Characteristic of charge accumulation in glass materials under electron beam irradiation," Proceedings of the 8th Spacecraft Charging Technology Conference, Huntsville, AL, (2003).

[18] Osawa, N., S. Takahashi, Y. Tanaka, T. Takada, R. Watanabe, N. Tomita, V. Griseri, L. Levy, and C. Laurent, "Measurement of bulk charge in dielectric materials irradiated by electron beam in vacuum

environment," Proceedings of the 8th Spacecraft Charging Technology Conference, Huntsville, AL, (2003).

[19] Usui, Y., T. Sakai, M. Ishikawa, T. Isono, Y. Tanaka, T. Takada, R. Watanabe, N. Tomita, and Y. Murooka, "Measurement of charge distribution in electron beam irradiated PMMA using electro-optical effect," Proceedings of the 8th Spacecraft Charging Technology Conference, Huntsville, AL, (2003).

[20] Tatsuo Takada, "Pulse Acoustic Technology for Measurement of Charge Distribution in Dielectric Materials for Spacecraft," Proceedings of the 9th Spacecraft Charging Technology Conference, (EPOCHAL TSUKUBA, TSUKUBA, April 4-8, 2005).

[21] Davies, R. E., Measurement of Angle-resolved Secondary Electron Spectra, PhD Dissertation, Utah State University, 1999.

[22] Chang, W. Y, J. R. Dennison, J. Kite, and R. E. Davies, "Effects of evolving surface contamination on spacecraft charging," Proceedings of the 38th American Institute of Aeronautics and Astronomics Meeting on Aerospace Sciences, Reno, NV (2000b).

[23] C.D. Thompson, V. Zavyalov, J.R. Dennison, J. Corbridge, "Electron Emission Properties of Insulator Materials Pertinent to the International Space Station," Proc. of the 8th Spacecraft Charging Tech. Conf., (Huntsville, AL, USA), 2004.

[24] C.D. Thomson, V. Zavyalov, J.R. Dennison, "Instrumentation for studies of electron emission and charging from insulators," Proc. of the 8th Spacecraft Charging Tech. Conf., (Huntsville, AL, USA), 2004.

[25] T. Schneider, NASA Marshall Space Flight Center, Materials, Processes, and Manufacturing Department, (private communications), 2003.

[26] N.R. Whetten, J.Appl. Phys. 35, 3279 (1964).

[27] P.H. Dawson, "Secondary Electron Emission Yields of Some Ceramics," J. Appl. Phys. 35, 3644 (1966)

[28] N.W. Green, JR Dennison, "Deep Dielectric Charging of Spacecraft Polymers by Energetic Protons," Proc. of the 10th Spacecraft Charging Tech. Conf., (Biarritz, France), 2007